Basis Function Sampling: A New Paradigm for Material Property Computation

Jonathan K. Whitmer, Chi-cheng Chiu, Abhijeet A. Joshi, and Juan J. de Pablo

Phys. Rev. Lett. **113**, 190602 — Published 7 November 2014

DOI: 10.1103/PhysRevLett.113.190602

Basis Function Sampling: A New Paradigm for Material Property Computations

Jonathan K. Whitmer,[1, 2, *] Chi-cheng Chiu,[1, 2] Abhijeet A. Joshi,[3] and Juan J. de Pablo[1, 2]

[1] *Institute for Molecular Engineering, University of Chicago, Chicago, Illinois 60637*
[2] *Materials Science Division, Argonne National Laboratory, Argonne, Illinois 60439*
[3] *Department of Chemical and Biological Engineering, University of Wisconsin-Madison, Madison, WI 53706-1691*

Wang–Landau sampling, and the associated class of flat histogram simulation methods have been remarkably helpful for calculations of the free energy in a wide variety of physical systems. Practically, convergence of these calculations to a target free energy surface is hampered by reliance on parameters which are unknown *a priori*. Here, we derive and implement a method built upon orthogonal functions which is fast, parameter-free, and (importantly) geometrically robust. The method is shown to be highly effective in achieving convergence. An important feature of this method is its ability to attain arbitrary levels of description for the free energy. It is thus ideally suited to *in silico* measurement of elastic moduli and other material properties related to free energy perturbations. We demonstrate the utility of such applications by applying our method to calculate the Frank elastic constants of the Lebwohl–Lasher model of liquid crystals.

Free energies provide essential information about the properties and structure of materials, including self-assembled colloidal clusters [1], crystals [2], and folded protein states [3]. Calculations of the free energy are challenging, particularly when the associated landscape exhibits large, rapidly varying features [4]. Many methods have been proposed to calculate free energies in simulations of many-body systems. Examples include - but are not limited to - thermodynamic integration [5, 6], adaptive bias potentials [7–12], parallel tempering coupled to histogram reweighting [13–16], density-of-states sampling [17–19], nonequilibrium steered dynamics exploiting Jarzynski's identity [20, 21], expanded ensemble [22–24], and flux-based methods [25–27]. Expanded ensemble calculations, which extract free energies by enforcing uniform sampling on a small set of thermodynamic quantities, are of particular interest for their efficiency and wide application [24]. These methods may naturally measure the free energetic cost of perturbations [28], codified by material properties defining response to (e.g.) thermal stress, tension, torsion or shear by probing the local free energy topography along a deformation coordinate ξ,

$$F(\xi) = F_0 + F_1\xi + \frac{1}{2}F_2\xi^2 + \dots \,. \tag{1}$$

Such polynomial (Taylor) expansions are ubiquitous in physical models. Here, we demonstrate that such expansions may be exploited by targeted sampling along a set of orthogonal polynomials $P_i(\xi)$, to determine the material properties F_i. We denote this method of free energy calculation basis function sampling (BFS). Further, we show that adaptive biasing driven by a truncated set of orthogonal basis functions is broadly applicable, involves no *ad hoc* parameters, and naturally satisfies boundary conditions on the domain of interest. Importantly, we demonstrate that such methods greatly reduce errors in free energy calculations relative to the existing approaches based on Wang–Landau sampling.

Until recently, free energy calculations in molecular simulations required a connecting pathway between two states; through a combination of umbrella sampling (to resolve rare states) [29], histogram reweighting [13, 14] and thermodynamic integration techniques [29], the change in free energy during transformation between a pair of macrostates (denoted ξ_1 and ξ_2) could be obtained. This computation-intensive process has been supplemented over the past two decades with "flat histogram" or "density-of-states" methods, which directly determination of the density of states, or partition function, from a single simulation in computationally tractable fashion. One of these, Wang–Landau sampling (WLS) [17], calculates the density of states within energy (U) space by proposing random changes to the state, and biasing against visited energy levels. In contrast to the normal Metropolis criterion for Monte Carlo (MC) simulations, WLS performed in the multicanonical ensemble has an acceptance rate which is determined by the ratio of history dependent weight factors,

$$p(1 \to 2) = \min\left[W(\xi_1)/W(\xi_2), 1\right] \,, \tag{2}$$

where states 1 and 2 are microstates with labels $\xi_1 = U(1)$ and $\xi_2 = U(2)$ respectively. Upon satisfying detailed balance [30], all states become equally visited. The biasing factor $W(U)$ is thus an on-the-fly estimator for $\Omega(U)$, the density of states.

Regarding the energy U as a thermodynamic potential, analogous algorithms for other ensembles result via Legendre transformation [31]. The Helmholtz free energy $F = U - TS$, will be referenced in what follows, though our discussion applies generically. The relative probability of two states in the multicanonical ensemble, $\Omega(U(1))/\Omega(U(2)) = e^{\Delta S_{12}}$ is replaced by the ratio of their Boltzmann factors, $P(\xi_1)/P(\xi_2) = e^{-\beta(F(\xi_1)-F(\xi_2))}$ [30]. The adaptive weight factors $W(\xi_i)$ normalize subsets of the Boltzmann distribution so that macrostates are be equally visited. The resulting acceptance and conver-

gence criteria for microstates i of macrostates ξ_i are thus

$$p(1 \to 2) = \min\left[\frac{W(\xi_1)}{W(\xi_2)} e^{-\beta(U(2)-U(1))}, 1\right] \quad (3)$$

$$\frac{e^{-\beta F(\xi_1)}}{W(\xi_1)} = \frac{e^{-\beta F(\xi_2)}}{W(\xi_2)} \quad (4)$$

Defining $\Phi = k_B T \log(W)$, Eq. 4 implies constant $F + \Phi$—the ratio of weight factors which previously codified entropy now codifies Helmholtz free energy. Updating W in this fashion is the basis for Expanded Ensemble Density of States (ExEDOS) [19, 30], joint density of states [32] and metadynamics [23, 24, 33] approaches. In them, one must identify a set of collective variables (CVs) $\vec{\xi}$ to characterize the system. The common choice of U results in $W(U) = \Omega(U)e^{-\beta U}$, equivalent to WLS. Many order parameters can prove useful, such as protein geometry, radius of gyration, nematic ordering, and coordination numbers.

A key idea here is the duality of the weighting factor, serving both as a measure of relative probability *and* a biasing potential Φ, computed on-the-fly. The second perspective is useful, as it allows connection of $\Phi(\vec{\xi})$ to the topography of the free energy surface (FES). In each visit to a particular macrostate, one deposits a 'sandhill' of bias. As the FES begins to fill, diffusion across free energy space becomes uninhibited, and the histogram becomes flat. Upon convergence, the potential Φ obtained in this manner is, up to a constant, $-F$. A set of distinct but similar methods, including Adaptive Bias Force [34], Adaptive Bias Potential [10], and Adaptive Umbrella Sampling [11] use the same principle to create a flat histogram, and thus obtain the FES. In general, these methods are not parameter free. The biasing potential approaches the true FES at a rate determined by diffusion, and by a set of parameters bespoke to each realization, such as the shape and amplitude of elemental biases [33, 35, 36]. The problems of each may be outlined by considering their role in continuous versions of WLS [32]. Including metadynamics, we collectively refer to these as CWLS.

CWLS methods are based on passing the discrete states of Eq. 2–4 to a continuum using Gaussian or similar biases; e.g. elemental biases $g(\vec{\xi}, \vec{s}_i)$ of the form

$$g(\vec{\xi}, \vec{s}_i) = W_i e^{-\frac{[\vec{\xi}-\vec{s}_i]^2}{2\sigma_i^2}}. \quad (5)$$

In this equation, the history of the system is indexed by i, with W_i the biasing weight, $\vec{s}_i$ the order parameter of configuraiton i, and σ_i the Gaussian width. The distinction between historical order parameters $\vec{s}_i$ and those on which we obtain the free energy $\vec{\xi}$ is a useful one. Functions $g(\vec{\xi}, \vec{s}_i)$ may be understood as an attempt to faithfully replicate an exact representation for the biasing potential on the overdetermined basis of δ-functions [30]. The smearing is beneficial, as it renders the resulting bias continuous and differentiable (though, for a counterpoint, see the Adaptive Bias Force method [34], which computes these forces directly from the underlying histogram). Problematically [cf. Fig 1(a)], this smearing is not always commensurate with domain boundaries. A variety of *ad hoc* methods have been created to remedy this problem, but no comprehensive solution exists [35, 37].

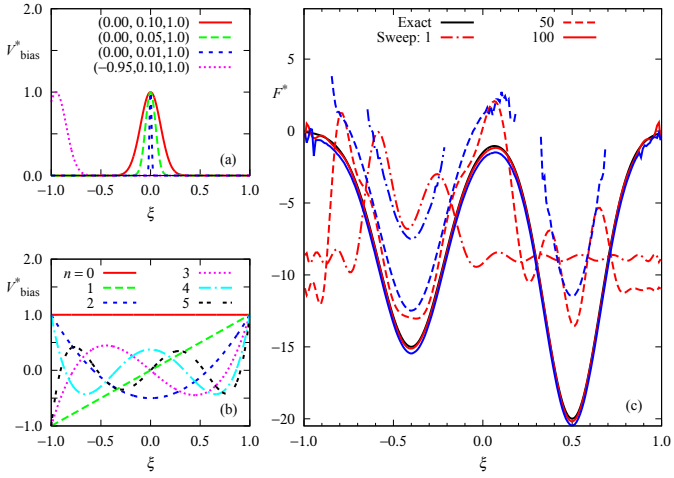

FIG. 1. Continuous methods for flat-histogram sampling utilize Gaussian biases (a) as a continuum approximant to the Dirac delta function. Plots are labeled (μ, σ, h) according to their center, width, and height. Near a wall, the finite width of a Gaussian leads a system to under-bias due to tail truncation. Pileup of these peaks leads to unphysical trapping and oversampling. (b) Projection onto orthogonal special functions [such as the Legendre polynomials $L_n(\xi)$] alleviates these issues. (c) Proof of concept for BFS within a one-dimensional double Gaussian well. The estimated free energy is projected onto a 25th-order Legendre polynomial expansion. Over 100 MC Sweeps, the polynomial bias drives exploration of phase space and self-refines until the histogram is flat and the bias and free energy have converged. The black curve denotes the exact underlying free energy, while red and blue curves are the on-the-fly free energy estimate and negative of the bias, respectively. A movie of the convergence is contained in the SM [30]

The discrete method (e.g., ExEDOS) contains, in addition to the time interval over which flatness is determined, a second input parameter that helps determine convergence—the bias deposition rate. CWLS introduces another, the Gaussian width σ. The desire for a parameter-free, accurate boundary method inspires our choice to replace the δ approximation (cf. Eq. 10 of SM [30]) with a local histogram approximating the partition function $Z(\xi)$, which is then projected onto a truncated set of orthogonal basis functions [cf. Fig 1(b)] able to represent any function on the CV domain Ξ to arbitrary accuracy. The result (BFS) is a parameter-free, robust method that enables direct measurement of material constants via the free-energetic cost of perturbation.

Many examples of normalized orthogonal special functions exist, including Fourier series, Bessel Functions, Chebyshev Polynomials, and Hermite Polynomials. These are sets of functions $\{f_i\}$, defined on a domain Ξ relative to a kernel or weight function $w(\vec{\xi})$, such that

$$\int_\Xi f_i(\vec{\xi}) f_j(\vec{\xi}) w(\vec{\xi}) d\vec{\xi} = \delta_{ij} c_j \ , \tag{6}$$

with c_j a normalization constant. This property means that any function ϕ defined on the domain Ξ may be represented as an expansion

$$\phi(\vec{\xi}) = \Sigma_i \alpha_i f_i(\vec{\xi}) \ , \tag{7}$$

$$\alpha_i = \frac{1}{c_i} \int_\Xi \phi(\vec{\xi}) f_i(\vec{\xi}) w(\vec{\xi}) d\vec{\xi} \ . \tag{8}$$

When the sum over i is truncated at a maximum N, the result is an approximation to the overall function. We will use these properties to construct an estimate Φ to the negative of the Helmholtz free energy F. In what follows, we work along a single CV ξ, and utilize the Legendre polynomials L_i. These have the attractive feature that $w(\xi) = 1$, and are defined on the interval $[-1, 1]$.

Simulations proceed in stages (sweeps), where the bias applied within sweep i is denoted by Φ_i. We start with $\Phi_0 = 0$ so that simulations proceed according to the unbiased Metropolis criterion. Each time a microstate j is visited, the order parameter $s_j = \xi(\vec{x}_j)$ is calculated, and recorded in a histogram $H_i(\xi)$. This proceeds for $N_{\text{step},i}$ MC steps, after which the histogram is converted to an unbiased estimator for the partition function

$$\tilde{H}_i(\xi) = H_i(\xi) e^{\beta \Phi_i(\xi)} \ . \tag{9}$$

This quantity may be directly converted into a bias through $\Phi_{i+1} = -\beta F_i = \log(\tilde{H}_i)$. However, this is not very useful if the current bias does not permit sampling on the full domain Ξ. Often, it is not known *a priori* if the system state will diffuse over the entire domain, and $N_{\text{step},i}$ may be adjusted after each sweep [see Supplementary Material (SM) [30]]. Historical information is then accrued in the partition function estimate:

$$Z_i(\xi) = \Sigma_{j \le i} W(t_j) \tilde{H}_j(\xi) \ . \tag{10}$$

The weight function $W(t_j)$ determines how sampling history enters the average. Our simulations primarily utilize the prescription $W(t_j) = N_{\text{step},j}$, though this may be adjusted further to bias the estimates toward recent information and enhance convergence. The bias potential $-\beta F_i(\xi) = \log(Z_i(\xi))$ is then projected onto a truncated basis,

$$\beta \Phi_{i+1}(\xi) = \Sigma_j^N \alpha_j^i L_j(\xi), \tag{11}$$

$$\alpha_j^i = \frac{2}{2i+1} \int_{-1}^{1} \log(Z_i(\xi)) L_j(\xi) d\xi \ . \tag{12}$$

The process is repeated until the free energy has converged, as determined by evolution of the coefficients α_j^i. This process is closely related to those obtaining a flat histogram via fitting parameters, as in Refs. [7, 11], with the distinction that projection to orthogonal functions implicitly defines the best approximation to the FES at order N, and may be adapted on-the-fly with minimal numerical overhead.

This algorithm naturally contains two parameters affecting convergence. One is the length of the sampling interval, while the other is the number of basis functions onto which the free energy is projected. These affect only the rate of convergence, and not the accuracy of the converged free energy, in contrast to the W_i and σ_i parameters of CWLS, which set the roughness of final free energy estimates and must be adequately tempered [33, 38] to remove such effects. The first parameter plagues all flat histogram methods; sampling is determined by the rate of diffusion in the system, and one cannot in general tell if a system is stuck in a free energy basin, or is merely diffusing extremely slowly. The second input parameter is just a convenient choice. The number of coefficients may be adjusted during a given simulation to enhance sampling. Thus, we have constructed a flat-histogram method which is free of ad hoc parameters. Importantly, the resulting bias function is smooth and may be easily applied in molecular dynamics simulation.

A proof-of-concept using a double-welled Gaussian potential is shown in Fig 1(c). Details of this simulation are given in the SM [30]. Within 100 iterations, the differences between the applied bias, estimated free energy $-\log(Z_i(\xi))$, and known free energy are negligible. Once sampling is sufficient to cover the domain of ξ, convergence proceeds rapidly. Importantly, the difference between the free energy estimate $F_i(\xi)$ and the bias potential $-\Phi(\xi)$ is dominated by contributions from the $(N+1)$th order polynomial [30], but is otherwise flat. Direct comparison using this example shows that while initial convergence is facilitated by ExEDOS sampling, the Basis Function method eventually overtakes ExEDOS in accuracy; moreover, it does so without the need to tweak and optimize biasing parameters before and during the calculation [30].

Two additional examples are explored in Figure 2, which compares the efficacy of the ExEDOS and BFS methods. Panel (a) plots the PMF (including entropic effects) between two Lennard-Jones particles versus the analytical result [30]. With the chosen parameters, each converges within eight sweeps. For ExEDOS, this may be tuned by clever adjustment of the initial bias and sampling interval using *a priori* knowledge of the FES; for BFS, this is unnecessary. Moving up in complexity, we examine the phase behavior of the Lebwohl–Lasher (LL) liquid crystal model model [30]. Though density of states simulations have been performed on this system [39], an analytical solution for the density of states

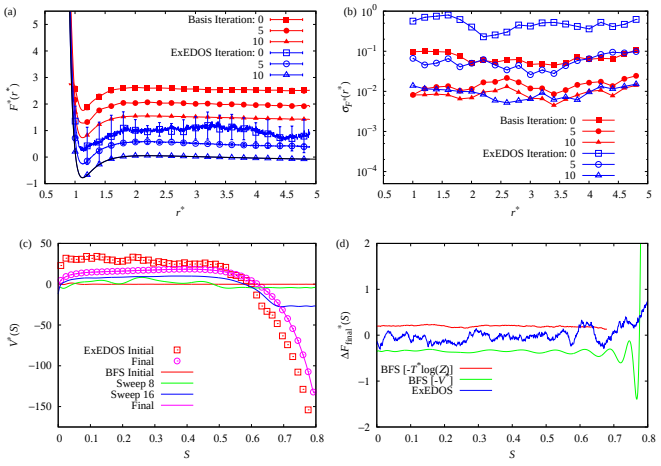

FIG. 2. (a) Potential of mean force between two Lennard-Jones particles in ExEDOS and BFS methods averaged over 10 independent runs. Here, indivdual ExEDOS sweeps are 10× longer than BFS sweeps [30]. Each simulation converges to the analytical result within 10 sweeps. Data are offset by 5 energy units for clarity, with solid black lines showing the agreement between the analytical potential and simulation results. While ExEDOS methods promote more initial exploration, the standard deviation σ_{F^*} plotted in panel (b) demonstrates quick convergence for BFS relative to ExEDOS. (c,d) Comparisons of free energy (plotted using the bias potential V^*) for ExEDOS and BFS simulations of a $10\times10\times10$ LL model, run for equal CPU time with parameters given in the SM [30]. ExEDOS is seen again to promote initial sampling, but features large fluctuations throughout the free energy surface, defined by $F_i^* - F_{i-1}^*$, in contrast to BFS which smoothly converges away from the $\approx 150 k_{\rm B}T$ wall at the boundary of S. Differences in both the final bias $-V^*_{\rm final}$ and estimated free energy $-T^*\log(Z_{\rm final})$ away from the boundary are plotted.

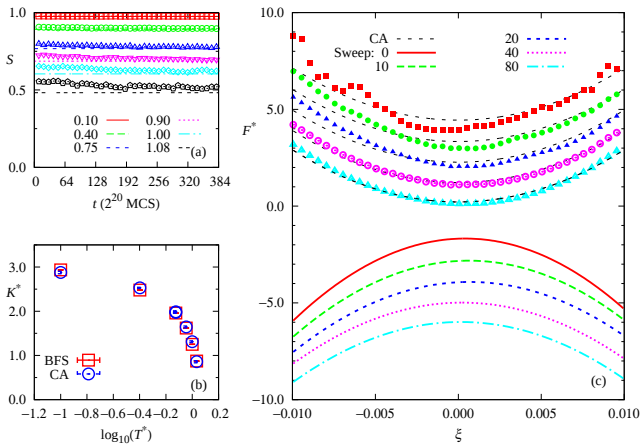

FIG. 3. Liquid crystal material constants simulations by BFS for the Lebwohl–Lasher model on an $L = 32$ cubic lattice. (a) To sample ξ effectively, it is necessary to properly equilibrate the system; here we show the relaxation of this model [30] as a function of time, measured in Monte Carlo steps (MCS). Symbols correspond to a typical simulation, with colored lines the bulk value from Ref [42]. (b) Measurements of the dimensionless elastic constant K^* [30] agree with the results of Ref. [42] (CA). (c) A sequence of free energy surfaces for $T^* = 0.90$ shows how convergence is approached, through the gradual application of bias permitting sampling of unfavorable states near the edge of the interval. Multiple-walker BFS [30] is utilized to overcome slow diffusion in the deformation coordinate. Upper curves are the measured free energy, while lower curves denote the applied bias. The curves have been offset for clarity, with the dashed black lines corresponding to the elastic constant of Ref. [42].

is not available. Fig. 2(b,c) demonstrate that both ExEDOS and BFS methods converge to the underlying free energy $F(S)$. Similar to the previous examples, ExEDOS results in faster initial sampling relative to BFS, though BFS attains much higher accuracy away from the $\approx 150 k_{\rm B}T$ barrier at high nematic order parameter S; this holds for each direct comparison we have performed (cf. Section II of SM [30]). By contrast, BFS converges over most of the region of interest quickly, and spends later times filling in rare states. This presents BFS as a fast, robust method for estimating free energy surfaces. Importantly, by managing the regions of interest, using multiple walkers [40, 41], and combining statistics using (e.g.) WHAM [13, 14], one may quickly converge the FES of larger domains that prohibit fast diffusion.

Finally, we highlight a benefit unique to BFS. The orthogonal expansion allows truncation at arbitrary order to study the effects of perturbations on the free energy of a system (Eq. 1), and thus determine material constants. In Fig 4(a–c), we show three deformations corresponding to bend, twist, and splay, whose elastic coefficients are k_{33}, k_{22}, and k_{11}, respectively. Obtaining these constants by traditional techniques is notoriously challenging [28, 42]. Utilizing the fundamental bend, twist and splay modes (cf. Fig. 4) [43], we may excite a single deformation using expressions outlined in the SM [30].

The details of the LL model set the values of k_{ii} equal to a constant, K (non-dimensionalized as K^* [30]). Utilizing a recently devised method for generating fundamental bend, twist, and splay elastic perturbations *in silico* [28], we define an order parameter ξ corresponding to bend, splay, or twist. The resulting free energy profile is $F^*(\xi) = V^*K^*\xi^2/2$, with V^* the reduced system volume, which is equal to the number of spins. An expansion (Eq. 12) truncated above L_2 is used to extract elastic coefficients. Our simulations are summarized in Figure 3. After a significant period of equilibration [cf. Fig. 3(a)] we proceed with the BFS algorithm. A typical path to convergence is depicted in Fig. 3(c). The resulting coefficients, plotted in Fig. 3(b) match identically with previous investigations based on long-wavelength director fluctuations [42].

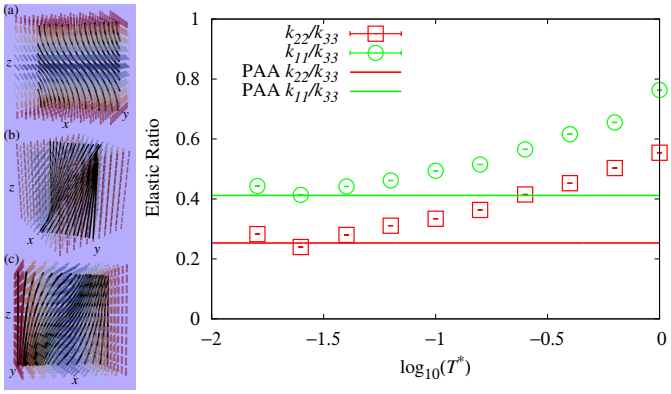

FIG. 4. The extended Lebwohl–Lasher model of Ref. [44] splits the elastic constants of bend, twist and splay deformations (diagrams at left). The elastic ratios of these coefficients (determined by BFS) for a model representing para-azoxyanisole (PAA) are given in the plot at right, with the expected ratios recovered as temperature is quenched toward zero [30].

Expanding on this result, in Fig. 4 we show that our method also captures the elastic ratios associated with generalized LL models; the model considered here was derived to describe para-azoxyanisole (PAA) in the limit of zero temperature [30, 44]. Our simulations clearly obtain the correct elastic anisotropy at low T^*, with logarithmic growth in both ratios approaching the isotropic–nematic transition. This type of measurement opens new possibilities for *in silico* determination of compressional, shear, and torsional elastic moduli of solids, along with liquid crystal deformations.

In conclusion, we have introduced a parameter-free flat histogram method for free energy calculations. Coupling this method to currently available umbrella sampling and parallel replica exchange techniques allows one to obtain arbitrary free energy surfaces from a set of basis function simulations on defined intervals. This method is geometrically robust, and permits the direct measurement of material constants defining the systemic response to free energy perturbations.

We wish to thank S. Singh, M. McGovern and T. F. Roberts for helpful discussions. We gratefully acknowledge computational resources accessible through the University of Chicago Midway cluster, and the Blues cluster operated by the Laboratory Computing Resource Center (LCRC) at Argonne National Laboratory. The algorithm development presented in this work is supported by the U.S. Department of Energy, Basic Energy Sciences. The calculation of elastic constants of liquid crystals is supported by the University of Wisconsin Materials Research Science and Engineering Center (UW-MRSEC) under National Science Foundation Grant No. DMR-1121288.

* Current Address: Department of Chemical and Biomolecular Engineering, University of Notre Dame, Notre Dame, Indiana 46556

[1] G. Meng, N. Arkus, M. P. Brenner, and V. N. Manoharan, Science **327**, 560 (2010).

[2] A. D. Bruce, A. N. Jackson, G. J. Ackland, and N. B. Wilding, Phys. Rev. E **61**, 906 (2000).

[3] A. Barducci, R. Chelli, P. Procacci, V. Schettino, F. L. Gervasio, and M. Parrinello, J. Am. Chem. Soc. **128**, 2705 (2006).

[4] J. N. Onuchic, Z. Luthey-Schulten, and P. G. Wolynes, Ann. Rev. Phys. Chem. **48**, 545 (1997).

[5] E. Carter, G. Ciccotti, J. T. Hynes, and R. Kapral, Chem. Phys. Lett. **156**, 472 (1989).

[6] M. Sprik and G. Ciccotti, J. Chem. Phys. **109**, 7737 (1998).

[7] B. A. Berg and T. Neuhaus, Physics Letters B **267**, 249 (1991); Phys. Rev. Lett. **68**, 9 (1992); B. A. Berg, Int. J. Mod. Phys. C **03**, 1083 (1992).

[8] A. P. Lyubartsev, A. A. Martsinovski, S. V. Shevkunov, and P. N. Vorontsov-Velyaminov, J. Chem. Phys. **96**, 1776 (1992).

[9] T. Huber, A. E. Torda, and W. F. van Gunsteren, J. Comput. Aided Mol. Des. **8**, 695 (1994).

[10] B. M. Dickson, F. Legoll, T. Lelièvre, G. Stoltz, and P. Fleurat-Lessard, J. Phys. Chem. B **114**, 5823 (2010).

[11] C. Bartels and M. Karplus, J. Comp. Chem. **18**, 1450 (1997).

[12] T. Lelièvre, M. Rousset, and G. Stoltz, J. Chem. Phys. **126**, 134111 (2007).

[13] S. Kumar, J. M. Rosenberg, D. Bouzida, R. H. Swendsen, and P. A. Kollman, J. Comp. Chem. **13**, 1011 (1992).

[14] S. Kumar, J. M. Rosenberg, D. Bouzida, R. H. Swendsen, and P. A. Kollman, J. Comp. Chem. **16**, 1339 (1995).

[15] Q. Yan and J. J. de Pablo, J. Chem. Phys. **111**, 9509 (1999).

[16] Y. Sugita and Y. Okamoto, Chem. Phys. Lett. **329**, 261 (2000).

[17] F. Wang and D. P. Landau, Phys. Rev. Lett. **86**, 2050 (2001).

[18] F. Wang and D. P. Landau, Physical Review E **64**, 056101 (2001).

[19] E. B. Kim, R. Faller, Q. Yan, N. L. Abbott, and J. J. de Pablo, J. Chem. Phys. **117**, 7781 (2002).

[20] C. Jarzynski, Phys. Rev. Lett. **78**, 2690 (1997).

[21] S. Park, F. Khalili-Araghi, E. Tajkhorshid, and K. Schulten, J. Chem. Phys. **119**, 3559 (2003).

[22] F. A. Escobedo and F. J. Martinez-Veracoechea, J. Chem. Phys. **129**, 154107 (2008).

[23] A. Laio and M. Parrinello, Proc. Natl. Acad. Sci. (U. S. A.) **99**, 12562 (2002).

[24] A. Laio and F. L. Gervasio, Rep. Prog. Phys. **71**, 126601 (2008).

[25] S. Singh, C.-c. Chiu, and J. J. Pablo, J. Stat. Phys. **145**, 932 (2011).

[26] S. Singh, C.-c. Chiu, and J. J. de Pablo, J. Chem. Theory Comput. **8**, 4657 (2012).

[27] S. Trebst, D. A. Huse, and M. Troyer, Phys. Rev. E **70**, 046701 (2004).

[28] A. A. Joshi, J. K. Whitmer, O. Guzmán, N. L. Abbott, and J. J. de Pablo, Soft Matt. **10**, 882 (2014).

[29] D. Frenkel and B. Smit, *Understanding Molecular Simulation*, 2nd ed. (Academic Press, San Diego, 2002).

[30] Supplementary Material including further method details, expanded discussion, and simulation parameters are available online at XXX.

[31] D. Chandler, *Introduction to Modern Statistical Mechanics* (Oxford University Press, Oxford, U.K., 1987).

[32] C. Zhou, T. C. Schulthess, S. Torbrügge, and D. P. Landau, Phys. Rev. Lett. **96**, 120201 (2006).

[33] A. Barducci, G. Bussi, and M. Parrinello, Phys. Rev. Lett. **100**, 020603 (2008).

[34] E. Darve, D. Rodríguez-Gómez, and A. Pohorille, J. Chem. Phys. **128**, 144120 (2008).

[35] M. McGovern and J. J. de Pablo, J. Chem. Phys. **139**, 084102 (2013).

[36] D. Branduardi, G. Bussi, and M. Parrinello, J. Chem. Theory Comput. **8**, 2247 (2012).

[37] Y. Crespo, F. Marinelli, F. Pietrucci, and A. Laio, Phys. Rev. E **81**, 055701 (2010).

[38] F. Liang, J. Stat. Phys. **122**, 511 (2006).

[39] R. Shekhar, J. K. Whitmer, R. Malshe, J. A. Moreno-Razo, T. F. Roberts, and J. J. de Pablo, J. Chem. Phys. **136**, 234503 (2012).

[40] L. Janosi and M. Doxastakis, J. Chem. Phys. **131**, 054105 (2009).

[41] P. Raiteri, A. Laio, F. L. Gervasio, C. Micheletti, and M. Parrinello, J. Phys. Chem. B **110**, 3533 (2006).

[42] D. J. Cleaver and M. P. Allen, Phys. Rev. A **43**, 1918 (1991).

[43] F. C. Frank, Disc. Farad. Soc. **25**, 19 (1958).

[44] G. R. Luckhurst and S. Romano, Liq. Cryst. **26**, 871 (1999).